Journal of Materials Chemistry A

PAPER

The effects of Ta_2O_5–ZnO films as cathodic buffer layers in inverted polymer solar cells

Cite this: *J. Mater. Chem. A*, 2014, **2**, 9361

Jo-Lin Lan,[a] Sheng-Jye Cherng,[a] Yi-Hsun Yang,[a] Qifeng Zhang,[a] Selvam Subramaniyan,[b] Fumio S. Ohuchi,[a] Samson A. Jenekhe[b] and Guozhong Cao*[a]

Received 19th March 2014
Accepted 16th April 2014

DOI: 10.1039/c4ta01350f

www.rsc.org/MaterialsA

Ta_2O_5–ZnO composite films with varied composition were fabricated by sol–gel processing and applied as cathodic buffer layers (CBLs) for inverted polymer solar cells, and demonstrated enhanced power conversion efficiency with excellent stability. Physical and surface properties of Ta_2O_5–ZnO CBL films were examined by XPS, AFM, UV-Vis absorption spectra, and goniometry. It was found that CBLs incorporated with Ta_2O_5 exert two competing impacts on the solar cell performances. On one hand, the presence of Ta_2O_5 is likely to induce more positive charges around the Zn atom and form Ta–O–Zn bonding; it can reduce the surface charge recombination between the bulk heterojunction (BHJ) active layer and the cathodic buffer layer (CBL), and result in high power conversion efficiency; however, on the other hand an excessive amount of Ta_2O_5 would block the pathways of charge transport and lead to a drastic reduction in power conversion efficiency.

Introduction

Organic photovoltaic (OPV) devices have attracted significant attention because of their acceptable energy conversion efficiency, potential to furnish low cost solar electricity, and capability to achieve portable application.[1–5] A conventional structure of OPVs (Fig. 1(a)) consists of a bulk heterojunction (BHJ) active layer made by blending a p-type polymer donor[6–8] with an n-type fullerene acceptor[9,10] on the top of indium tin oxide (ITO) glass modified by the hole transporting layer (HTL), such as poly(3,4 ethylenedioxylenethiophene):poly(styrene sulfonic acid) (PEDOT:PSS), molybdenum oxide (MoO_x), *etc.*,[11–14] and a low work function metal serving as the top electrode, typically aluminum, deposited on the top of the active layer. The most widely studied polymer:fullerene system is based on a solution processed p-type poly(3-hexylthiophene)(P3HT) polymer and an n-type [6,6]-phenyl-C_{61}-butyric acid methyl ester ($PC_{61}BM$) fullerene; the highest efficiency of this system is around 5%.[3,10,15] By designing low band gap polymer material that can absorb a broader solar spectrum, controlling the microstructure of the BHJ active layer to lengthen exciton diffusion length, and optimizing the device structure efficiency as high as 10% was reported recently.[16]

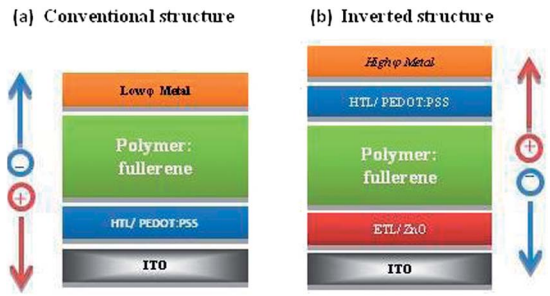

Fig. 1 (a) Conventional structure and (b) inverted structure of OPVs.

In spite of the dramatic improvement in power conversion efficiency and all the promising advantages, the conventional structure OPVs have a fatal weakness, *i.e.* a rapid performance degradation due to the low work function top metal electrode, and an unstable interface between the ITO substrate and HTL;[17–19] such a rapid performance degradation is unacceptable for any practical application. Therefore, the inverted structure OPV was proposed and studied to circumvent this drawback and demonstrated much improved performance stability.[20]

Comparing with the conventional structure OPVs, the charge flow path is opposite to that in the inverted one. Fig. 1(b) depicts the inverted OPV's structure. A cathodic buffer layer (CBL), usually a metal oxide such as ZnO, TiO_x, Nb_2O_5, Cs_2CO_3, or Al_2O_3,[14,21–25] is deposited on ITO glass to reduce its work function in order to lower the barrier for electron transfer to the ITO electrode. In addition, this kind of metal oxide needs to have hole blocking and electron collecting ability to enhance the power conversion efficiency.[26] The top electrode is replaced by a high work function metal, such as silver, to fulfill hole collection. The entire inverted structure is: ITO glass/metal oxide layer/(BHJ) active layer/hole transporting layer (HTL)/Ag. The mechanism by which the inverted structure OPVs have

[a]*Department of Material Science and Engineering, University of Washington, Seattle, WA, 98195, USA. E-mail: gzcao@u.washington.edu*

[b]*Department of Chemical Engineering, University of Washington, Seattle, WA, 98195, USA*

improved device stability is twofold: (1) the air sensitive, low work function top electrode (aluminum) is replaced with a stable, high work function metal, either silver or gold, and (2) the interface between the acidic PEDOT:PSS hole transporting layer and ITO glass is eliminated from the device.

Although inverted OPVs can improve device stability, they suffer from relatively low power conversion efficiency, possibly because of the electron loss on the interface between the BHJ active layer and the metal oxide layer such as slow charge injection due to work function alignment and electron traps on the CBL's surface defects.[27–30] For this reason, a lot of studies focus on the surface modification of metal oxide with self-assembled monolayers, such as C_{60}-SAMs, saline, C_{60} molecules, and ethoxylated polyethylenimine (PEIE),[31–35] manipulating its morphology and surface energy,[23,36] and new material doping to enhance its electron collecting ability, such as Al-doped ZnO, Ga-doped ZnO, zinc tin oxide, and $SrTiO_3$:ZnO.[37–41]

In this paper, we try to modify zinc oxide (ZnO) by introducing tantalum pentoxide (Ta_2O_5) as cathodic buffer layers (CBLs) for inverted structure OPVs. ZnO is an n-type semiconductor with a wide band gap of 3.3 eV and exhibits attractive features such as high electron mobility, good optical transmittance, and excellent stability.[42–45] Unfortunately, surface defect and easy formation of oxygen vacancies at the grain boundaries of ZnO often results in low conductivity of CBLs.[27–29,46,47] Tantalum pentoxide, on the other hand, is known for its high dielectric constant and index of refraction, and has found a variety of applications in electronics such as tantalum capacitors for its high dielectric constant,[48] antireflection coating for solar cells application due to its high refractive index and a low absorption coefficient (less than 10^3 cm^{-1}) for light,[49] and high-k dielectric for DRAM capacitor application.[50]

By applying Ta_2O_5–ZnO as the cathodic buffer layer (CBL), a possible mechanism was proposed to explain the relation between CBL composition, surface morphology, surface energy, and surface defect to photo-to-electrical energy conversion. PSEHTT/$PC_{71}BM$ was also studied as the BHJ active layer instead of P3HT/$PC_{61}BM$ in inverted OPVs, and the long-term stability of unencapsulated inverted OPVs under ambient conditions were also examined.

Experimental

Materials

Regioregular poly(3-hexylthiophene)(P3HT, 4002-E grade) was purchased from Rieke Metals, Inc. [6,6]-Phenyl-C_{61}-butyric acid methyl ester ($PC_{61}BM$, 99.0% purity) was purchased from American Dye Source, Inc. Poly(3,4-ethylenedioxylenethiophene):poly(styrene sulfonic acid) (PEDOT:PSS, Clevios 4083) was purchased from H. C. Starck. Poly[(4,4′-bis(2-ethylhexyl)dithieno[3,2-*b*:2′,3′-*d*]silole)-2,6-diyl-*alt*-(2,5-bis(3-(2-ethylhexyl)thiophen-2-yl)thiazolo[5,4-*d*]thiazole)] (PSEHTT) and [6,6]-phenyl-C_{71}-butyric acid methyl ester ($PC_{71}BM$) were synthesized by Prof. Jenekhe's group. Zinc acetate ($Zn(CH_3COO)_2$, 98.0%), 2-methoxyethanol ($CH_3OCH_2CH_2OH$, 99.0%), monoethanolamine ($NH_2CH_2CH_2OH$–$2H_2O$, 99.0%), tantalum(v) ethoxide ($Ta(OC_2H_5)_5$, 99.98%), ethanol (CH_3CH_2OH, 99.5%, 200 proof absolute), and acetic acid (CH_3COOH, 99.7%) were purchased from Sigma-Aldrich. All the chemicals were used as received without further purification. ITO glass (10–15 Ω sq^{-1}) substrates were purchased from Colorado Concept Coatings LLC. Samples were prepared on ITO substrates (1.5 × 1.5 cm^2), which were cleaned prior to use by ultrasonic agitation in a detergent solution, acetone, and isopropyl alcohol, and then dried under nitrogen flow.

Preparation of the Ta_2O_5–ZnO cathodic buffer layers

ZnO sol preparation. Zinc acetate dehydrate was first dissolved in a mixture of 2-methoxy ethanol and monoethanolamine at room temperature. The concentration of zinc acetate was 0.1 M and the molar ratio of monoethanolamine to zinc acetate was 1 : 1. The resulting solution was stirred using a magnetic stirrer at 60 °C for 2 h to yield a homogeneous, clear, and transparent sol.

$Ta(OR)_x$ sol preparation. Tantalum(v) ethoxide was first diluted in ethanol at room temperature, and then acetic acid was added to form a homogeneous, clear, and transparent sol. The final concentration of tantalum(v) was 0.1 M.

$Ta(OR)_x$–ZnO sol preparation. Both the $Ta(OR)_x$ and the ZnO sol concentrations were 0.1 M, and these two sols were simply mixed with molar ratio ($Ta(OR)_x$: ZnO = 0 : 100, 6 : 84, 12 : 82, 18 : 82, 24 : 76, 30 : 70, 100 : 0) to form a Ta_2O_5–ZnO sol.

The Ta_2O_5–ZnO sols were spin-coated after the prepared solution was aged at room temperature for one day in order to make it more glutinous. The sols were dropped onto ITO glass substrates, which were then spun twice at 3000 rpm for 30 s. After processing, the samples were immediately baked at 300 °C for 10 min and subsequently annealed at 350 °C for 20 min in air to convert to metal oxide. Throughout the device fabrication process, we fixed all the process parameters except the Ta_2O_5–ZnO sol composition.

Device fabrication

P3HT:$PC_{61}BM$ solution preparation. The chlorobenzene solution of P3HT:PCBM (1 : 0.8 by weight) containing P3HT (20 mg mL^{-1}) and PCBM (16 mg mL^{-1}) was stirred in a glovebox at 60 °C overnight. The solution was allowed to cool to room temperature and then filtered through a 0.2 μm polytetrafluoroethylene (PTFE) filter.

P3HT:$PC_{61}BM$ device. First, the P3HT:$PC_{61}BM$ blend solution was spin-coated onto the ITO substrates with the Ta_2O_5–ZnO buffer layer at 700 rpm for 30 s. Then the samples were baked at 225 °C for 1 min to help self-organization of P3HT, as well as to drive away residual solvent and assist the polymer contact with the Ta_2O_5–ZnO cathodic buffer layer. Then, the diluted PEDOT:PSS solution was spin-coated onto the active layer to form the hole-transport layer. The films were then baked at 120 °C for 10 min. A 100 nm thick Ag film was finally deposited under a vacuum of 2×10^{-6} Torr as the top electrode. The device structure of space-charge-limited-current (SCLC) measurement is the same only without the PEDOT:PSS layer.

PSEHTT:$PC_{71}BM$ solution preparation. PSEHTT/$PC_{71}BM$ blend solution with a composition of 1 : 2 ratio (w/w) was prepared by mixing 0.6 mL of the 6 mg mL^{-1} PSEHTT in

1,2-dichlorobenzene with 0.12 mL of the 60 mg mL^{-1} $PC_{71}BM$ in 1,2-dichlorobenzene and 2.5% (v/v) processing additive of 1,8-octanedithiol (ODT) in 1,2-dichlorobenzene and stirred for 10 min at 100 °C on a hot plate.

PSEHTT:$PC_{71}BM$ device. First, the PSEHTT/$PC_{71}BM$ blend solution was spin-coated onto the ITO substrates with the Ta_2O_5–ZnO buffer layer at 400 rpm for 40 s to form a 60–70 nm active layer. Then the samples were vacuum-dried for 30 min. After that, 7.5 nm MoO_3 and 120 nm Ag film were deposited under a vacuum of 2×10^{-6} Torr onto the active layer to form the hole-transport layer and top electrode.

I–V characterization

The *I–V* characteristics of the solar cell were tested in a glovebox using a Keithley 2400 source measurement unit and an Oriel Xenon lamp (450 W) coupled with an AM1.5 filter. A silicon solar cell certified by the national renewable energy laboratory (NREL) was used as a reference to calibrate the measurement conditions. The light intensity used in this study was 100 mW cm^{-2}.

Ta_2O_5–ZnO buffer layer characterization

The surface morphologies of the specimens were obtained using AFM (Asylum Research MFP-3D Stand Alone AFM) operated in tapping mode. Optical transmittance spectra were recorded using a Thermo Fisher Scientific (EVO30 PC) UV-vis recording spectrophotometer over the wavelength range between 300 and 900 nm. XPS spectra and secondary electron cutoff were generated using a PHI Versaprobe system with an Al Kα X-ray source and a 100 μm beam size. The work function value was calibrated with pure gold foil (5.1 eV). Measurements were taken while the sample was under ultrahigh vacuum (10^{-10} Torr). The contact angle was measured by goniometer, and each sample was measured four times in different areas.

Results and discussion

Power conversion efficiency of the inverted OPVs with P3HT:$PC_{61}BM$ as BHJ layer

Fig. 2 shows the *I–V* curves of the inverted OPVs with various Ta_2O_5–ZnO films as cathodic buffer layers (CBLs), and Table 1 summarizes the *I–V* characteristics based on the results presented in Fig. 2. Comparing pure ZnO CBL with a small amount of Ta_2O_5 (<18%) added, the fill factor is found to monotonically increase from 0.61 to 0.67 with an increase in the amount of Ta_2O_5, while both short circuit current density and open circuit voltage remain unchanged at 0.63 V and 9.7 mA cm^{-2}, respectively. As a result, the overall power conversion efficiency increases from 3.7% to a maximum of 4.12%. However, when the amount of Ta_2O_5 in the CBLs exceeds 24%, the power conversion efficiency reduces rapidly because of the sharp decrease of the fill factor. For the OPVs with pure Ta_2O_5 as the CBL, there is almost no detectable solar to electrical power conversion.

Such a change in power conversion efficiency with an increasing amount of Ta_2O_5 incorporated into the CBLs, first increasing to a maximum and then decreasing, indicates there

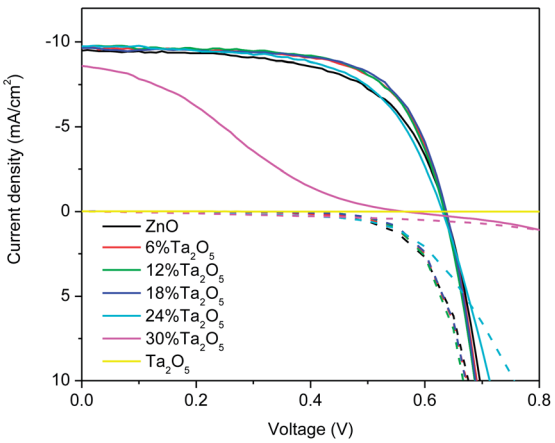

Fig. 2 The *I–V* curve at 1 sun and dark condition with various Ta_2O_5–ZnO films as the cathodic buffer layer. (BHJ active layer: P3HT:$PC_{61}BM$).

are two competing and opposite mechanisms in play. A closer look reveals that the short circuit current density and open circuit voltage remain constant with <24% Ta_2O_5–ZnO films as CBLs in inverted OPVs; however, there are some differences in the fill factor. The fill factor is known to be determined by series and shunt resistances of the solar cell device. The series resistance represents the overall series resistance and the shunt resistance is related to the recombination process in the device, respectively. As shown in Table 1, with a small amount of Ta_2O_5 (<18%) in CBLs, the series resistance stays at the same level, however, the shunt resistance gradually increases from 0.67 to 3.3 kΩ cm^2. The increase in shunt resistance suggests that the charge recombination is reduced. With further increasing the amount of Ta_2O_5 to 24% or 30%, the increase in series resistance becomes predominant, resulting in low power conversion efficiency.

In order to understand the possible mechanisms by which the Ta_2O_5–ZnO films as CBLs affect power conversion efficiency (PCE) of the inverted OPVs, the chemical and physical properties of the CBL were examined including transparency, morphology, surface energy, surface element composition, crystallinity, and electron mobility of Ta_2O_5–ZnO films.

Transparency of Ta_2O_5–ZnO films

Fig. 3 compares the UV-Vis absorption spectra of various Ta_2O_5–ZnO thin films, and it is clear that the UV-Vis absorption spectra

Table 1 *I–V* characteristics of inverted OPVs with various Ta_2O_5–ZnO CBLs (BHJ active layer: P3HT:$PC_{61}BM$)

	V_{oc} (V)	J_{sc} (mA cm^{-2})	FF	Efficiency (%)	R_{sh} (kΩ cm^2)	R_s (Ω cm^2)
Pure ZnO	0.636	9.49	0.613	3.70	0.67	8.72
6% Ta_2O_5	0.637	9.75	0.649	4.03	1	7.58
12% Ta_2O_5	0.634	9.73	0.661	4.08	5	7.20
18% Ta_2O_5	0.637	9.64	0.670	4.12	3.3	7.28
24% Ta_2O_5	0.631	9.75	0.616	3.79	1.67	10.07
30% Ta_2O_5	0.563	8.61	0.260	1.26	0.2	243.9
Pure Ta_2O_5	0.564	0.042	0.374	0.0009	11	125 000

have no significant difference regardless of the amount of Ta_2O_5. All the Ta_2O_5–ZnO films have good optical transmittance in the visible region with no appreciable antireflection effect with the incorporation of Ta_2O_5 in CBLs. It might be because the Ta_2O_5–ZnO film is very thin, only ~10 nm, and could be considered as completely transparent. Therefore, the introduction of various amounts of Ta_2O_5 in CBLs will not change its UV-Vis absorption spectra. Antireflection effect occurred when the thickness of Ta_2O_5 was up to 80 nm, as reported in literature.[49] Almost identical UV-Vis absorption spectra of CBLs with varied chemical composition suggest that the transmittance of the CBLs is not a determining factor affecting the power conversion efficiency.

Surface morphology and surface energy of Ta_2O_5–ZnO films

Fig. 4 shows the AFM and contact angle images of Ta_2O_5–ZnO films on ITO glasses. The root mean square (RMS) surface roughness and contact angle values are summarized in Table 2. It can be observed that the root mean square (RMS) value decreases when a small amount of Ta_2O_5 is blended into ZnO film (3.25 nm (pure ZnO) → 2.55 nm (6% Ta_2O_5)), and gradually increases with increasing Ta_2O_5 amount (2.55 nm (6% Ta_2O_5) → 3.05 nm (30% Ta_2O_5)). A smoother surface (with lower surface roughness) could be good for serving as CBLs for the inverted OPVs as it might allow better contact of the active polymer layer to the CBL.[23] However, it could not explain the fact that there is a significant drop of PCE when the amount of Ta_2O_5 varied from 18 to 30% in CBLs since the surface morphology does not show an appreciable difference. The contact angle of the films in the range of 50–55° does not show a detectable trend with varying the Ta_2O_5–ZnO composition, which means that the surface energy remains the same regardless of the addition of Ta_2O_5. All the films are slightly more hydrophilic compared with ITO glass.

Work function and surface chemical analysis of Ta_2O_5–ZnO films

Surface chemical analysis was carried out by X-ray photoelectron spectroscopy (XPS) (Fig. 5). Both the $Zn2p_{3/2}$ and

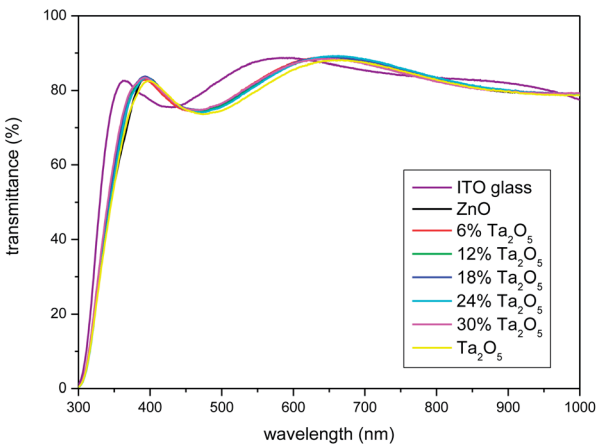

Fig. 3 The UV-vis spectra of ITO glass and various Ta_2O_5–ZnO/ITO glass.

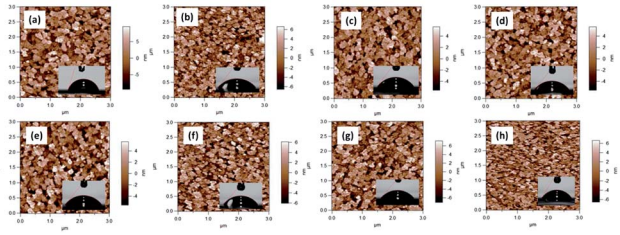

Fig. 4 The surface morphology and contact angle of various Ta_2O_5–ZnO/ITO glasses. (a) ITO glass; (b) ZnO; (c) 6% Ta_2O_5; (d) 12% Ta_2O_5; (e) 18% Ta_2O_5; (f) 24% Ta_2O_5; (g) 30% Ta_2O_5; (h) Ta_2O_5 on ITO glasses.

Ta4f data for each sample were scaled to the O1s emission intensity and shifted such that the O1s peaks had the same binding energy as 531 eV (this was necessary to account for charge neutralization and some surface contamination that suppressed the intensities of the peaks during transfer to the XPS system). For the $Ta4f_{7/2}$ and $Zn2p_{3/2}$ spectrum from the surfaces of the CBLs, their peaks are assigned as 26.35 and 1022.175 eV which represents Ta_2O_5 and ZnO.[51] The intensity of $Zn2p_{3/2}$ decreased with the addition of Ta_2O_5, whereas the intensity of Ta4f increased when the Ta_2O_5 concentration increased. As shown in Table 2, the peaks of $Zn2p_{3/2}$ shift to higher binding energy in the presence of Ta_2O_5, and it suggests that the Zn^{2+} cation may be transformed to $Zn^{(2+\delta)+}$ and this transfer could be accounted for by positively charged Ta^{5+}. When the concentration of Ta_2O_5 increased, $Zn2p_{3/2}$ peaks shift to higher binding energy; it can be proposed that Ta_2O_5–ZnO films do not only form as a physical mixture with two distinct Ta_2O_5 and ZnO phases, but form a chemical bond such as Ta–O–Zn in the system. If we correlate the XPS results with the PCE data, it can be proposed that more positive charge around Zn might benefit the electron transfer from the BHJ layer to the CBLs or lower the possibility of electron recombination occurring on the interface between the BHJ layer and CBLs.

The work function was calculated using the X-ray photoelectron spectroscopy (XPS) secondary electron cut off region, and is shown in Table 2. The work function of the Ta_2O_5–ZnO film fluctuated with chemical composition, first increasing with the addition of Ta_2O_5 from −4.9 eV for pure ZnO film to −4.69 eV (6%Ta_2O_5–ZnO), and gradually decreasing as more Ta_2O_5 was added. The high work function is favorable to electron transfer from the BHJ active layer to CBLs in the inverted polymer solar cell application,[35] however, the results obtained in the present investigation fell within the experimental error and demonstrated no direct relationship with the variation of power conversion efficiency. It definitely could not explain the fact that there was a significant drop of PCE in inverted OPVs with 24% and 30% Ta_2O_5–ZnO films used as CBLs.

Electron mobility and crystallinity of Ta_2O_5–ZnO films

Electron mobility can be determined by fitting the dark *I–V* curves for the single carrier devices with space-charge-limited-

Table 2 The root mean square (RMS) of surface roughness, contact angle, work function, XPS Zn $2p_{3/2}$ peaks position difference with pure ZnO (based on $Zn2p_{3/2}$ = 1022.175 eV) and electron mobility of various Ta_2O_5–ZnO/ITO glasses

	Roughness (nm)	Contact angle (°)	Work function (eV)	Δ binding energy (10^{-3} eV)	Electron mobility ($cm^2\ V^{-1}\ s^{-1}$)
ITO glass	4.42	71	−4.8	—	—
ZnO	3.25	52	−4.9	0	1.49×10^{-5}
6% Ta_2O_5	2.55	54	−4.69	63.6	1.67×10^{-5}
12% Ta_2O_5	2.63	54	−4.82	154.5	3.3×10^{-5}
18% Ta_2O_5	2.87	53.5	−4.91	295.3	2.3×10^{-5}
24% Ta_2O_5	3.05	55	−5.03	356.6	4.4×10^{-6}
30% Ta_2O_5	3.05	53	−4.94	388.4	1.1×10^{-7}
Ta_2O_5	3.36	60	−5.04	—	—

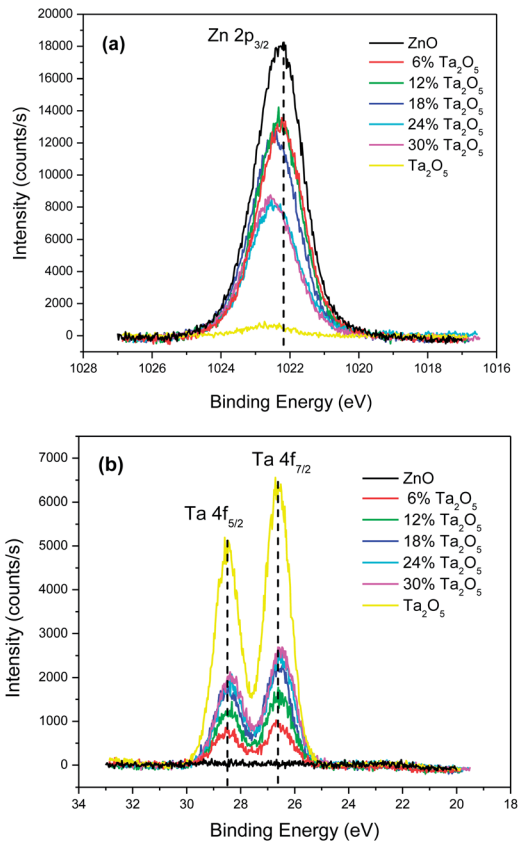

Fig. 5 XPS results of various Ta_2O_5–ZnO/ITO glasses. Core levels of (a) $Zn2p_{3/2}$ and (b) Ta 4f.

current (SCLC) model.[52] The electron-only structure of the device was ITO/Ta_2O_5–ZnO/P3HT:PCBM/Al fabricated to evaluate the electron mobility of Ta_2O_5–ZnO film by the charge transfer model of SCLC. The current is given by:

$$J = 9/8 \times \varepsilon_0 \times \varepsilon_r \times \mu_e \times V^2/D^3$$

where ε_0 is the permittivity of free space, ε_r is the relative permittivity of PCBM, μ_e is the electron mobility, and D is the thickness of the active layer. From Table 2, comparing with pure ZnO device (1.49×10^{-5} $cm^2\ V^{-1}\ s^{-1}$), the electron mobility of <18% Ta_2O_5–ZnO devices remains at the same level as pure ZnO ($\sim 10^{-5}$ $m^2\ V^{-1}\ s^{-1}$). While continuing the addition of Ta_2O_5, the electron mobility begin to drop drastically ($\sim 10^{-7}$ $m^2\ V^{-1}\ s^{-1}$), which correlates with the poor power conversion efficiency with 24% and 30%Ta_2O_5–ZnO films as CBLs.

Moreover, the crystallinity of 18% Ta_2O_5–ZnO and pure ZnO films were examined by XRD, and the results are shown in Fig. 6. NaCl was introduced by adding a drop of NaCl aqueous solution to the XRD samples and followed by crystallization at ambient conditions, and was used to detect any possible instrumental shift of the XRD peak positions. From Fig. 6, there is no signature peak representing Ta_2O_5, which means that Ta_2O_5 phase can not be detected by XRD and is more likely to form the amorphous phase. No shift existed of any ZnO XRD peaks in low and high diffraction angles; this result is a clear indication that there is no change of lattice constant in ZnO crystals further indicating that there is no incorporation of Ta ions into ZnO lattice. Moreover, the crystal size of these two films calculated by Scherrer equation are both 4.1 nm. It is very reasonable considering the fact that Zn^{2+} has a coordination number of 4 with an ionic radius of 60 pm, whereas Ta^{5+} typically has a coordination number of 6 with an ionic radius of 65 pm.[53] However, its ionic radius is more likely to be <35 pm when subjected to a coordination number of 4 and, thus, it is very unlikely that Ta^{5+} would

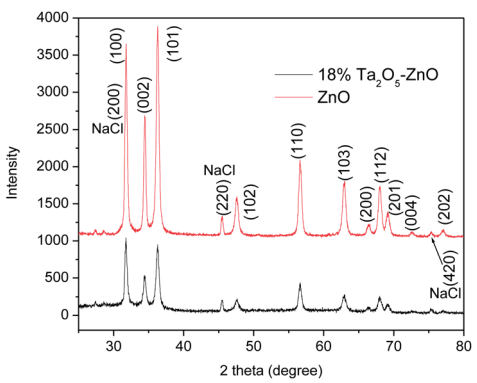

Fig. 6 XRD results of 18% Ta_2O_5–ZnO and ZnO film. Note that NaCl was added to the samples for XRD analyses and used as the reference to verify and confirm any possible change in lattice constants as a result of possible incorporation of Ta ions into ZnO crystals.

enter the ZnO crystal lattice. Moreover, the intensity of the ZnO peak enormously reduced when Ta_2O_5 was present, which suggests that part of ZnO may also become amorphous. Recalling the XPS results presented and discussed earlier in this paper, we have demonstrated that Ta–O–Zn chemical bonds unambiguously exist. The most reasonable explanation is that a fraction of ZnO formed an amorphous phase with Ta_2O_5 added to the film. Although it is not possible to determine the chemical composition and the volume fraction of such an amorphous phase, the amount of amorphous phase is likely to increase with an increased addition of Ta_2O_5 to the film. The presence of an amorphous phase and/or the small amount of crystalline ZnO will affect the electron transfer through CBLs, and result in low electron mobility, high series resistance, and small fill factor. When the amount of Ta_2O_5 in CBLs reaches a certain concentration, the amount of ZnO–Ta_2O_5 amorphous phase reaches such a volume fraction that forms an uncontinuous network with ZnO crystals embedded and separated by ZnO–Ta_2O_5 amorphous phase. Consequently, the electron transfer through ZnO percolated network is restricted, resulting in a drastic reduction in fill factor and power conversion efficiency. When Ta_2O_5 is used as a CBL, there is no detectable solar-to-electrical power conversion. It should be noted that this result is different from what was reported in an earlier paper[54] in which an inverted solar cell with Nb_2O_5 film as the CBL showed a ~3% power conversion efficiency. Although there is no clear explanation for such a discrepancy, Nb_2O_5 film (made with one spin-coating layer) reported in ref. 54 was presumably much thinner, half the thickness of the Ta_2O_5 film (two spin-coating layers), investigated in this study, while tunneling conduction decreases exponentially with increased thickness. In our previous work, the use of two spin-coating layers of Nb_2O_5 resulted in zero efficiency of the solar cell,[54] consistent with the Ta_2O_5 results presented here.

Furthermore, the improvement in fill factor might also be relative to the employment of different materials in CBLs and the change of the film's surface chemistry.[37–41] It was reported that ZnO grain defects play an important role in decreasing the electrical conductivity. There are numerous studies focusing on the low conductivity of thin ZnO layers in OPVs, and it results from the presence of adsorbed oxygen at its grain boundaries. The adsorbed oxygen can serve as an electron trap at these boundaries and therefore reduces the conductivity of these layers.[26,30,55] Therefore, both pure ZnO and 12% Ta_2O_5–ZnO films were annealing under oxygen or nitrogen atmosphere to simulate oxygen-rich or oxygen-barren in surface grain boundaries, and the results are shown in Table 3 and Fig. 7.

It was found that compared with processing under O_2 environment, the power conversion efficiency of the inverted OPVs with pure ZnO as CBLs was improved if it was annealed under N_2 atmosphere, which explains that the oxygen adsorbed in ZnO's grain boundaries can be removed if we apply the N_2 atmosphere to process our CBLs. However, for the inverted OPVs with 12% Ta_2O_5–ZnO films as CBLs, the power conversion efficiency remains the same when annealing in either O_2 or N_2 atmosphere. Although the exact mechanism to explain such insensitivity of Ta_2O_5–ZnO CBLs to O_2 and N_2 annealing is not known, this observation is likely to suggest that ZnO's surface grain boundaries and oxygen trapping sites are somehow covered by the Ta_2O_5 phase, or Ta_2O_5–ZnO becomes composite and has less surface grain boundaries to adsorb oxygen molecules. Ta_2O_5 is known for its high dielectric constant and it is also proposed that high dielectric constant material would favor the effective charge transfer in PSCs.[40,47] Applying high dielectric constant material as CBLs might form a spontaneous polarization to create an internal electric field while PSCs are in operation and reduce the electron recombination possibility,[40] which can also contribute to power conversion efficiency enhancement.

PSEHTT/$PC_{71}BM$ as BHJ active layer and long-term stability

In order to demonstrate the effect of Ta_2O_5–ZnO CBLs for the inverted OPVs with different BHJ systems, PSEHTT/$PC_{71}BM$ was applied as the active layer and replaced the commonly used P3HT/$PC_{61}BM$. PSEHTT is a kind of thiazolothiazole–

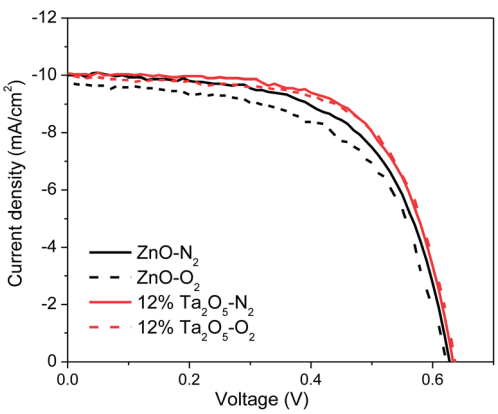

Fig. 7 The *I–V* curve at 1 sun with ZnO or 12%Ta_2O_5–ZnO films as the cathodic buffer layer (annealing under N_2 or O_2 atmosphere).

Table 3 *I–V* characteristics of inverted OPVs with various Ta_2O_5–ZnO CBLs (annealing under N_2 or O_2 atmosphere)

CBLs	Annealing atmosphere	V_{oc} (V)	J_{sc} (mA cm^{-2})	FF	Efficiency (%)
ZnO	N_2	0.63	9.99	0.61	3.82
	O_2	0.62	9.73	0.587	3.55
12% Ta_2O_5–ZnO	N_2	0.63	10.05	0.64	4.08
	O_2	0.64	9.99	0.64	4.06

dithienosilole copolymer semiconductor presented by Jenekhe's group in 2011, and achieved 5% power conversion efficiency in conventional structure OPVs at that time.[56] Inverted structure OPVs were prepared by combing PSEHTT/$PC_{71}BM$ and Ta_2O_5–ZnO CBLs, and the power conversion efficiency and *I–V* curves are summarized in Table 4 and Fig. 8. The highest efficiency is around 5.6% with 12% Ta_2O_5 film as CBLs, a 6% improvement compared with the 5.2% efficiency for pure ZnO as CBLs, which means that the Ta_2O_5–ZnO films as CBLs also work for PSEHTT/$PC_{71}BM$ systems to improve the overall power conversion efficiency. It should also be noted that the trend shown in Fig. 8 appears very similar to that in Fig. 2. When a small amount of Ta_2O_5 was added, the power conversion efficiency increased with the concentration of added Ta_2O_5, and then there was a drastic drop of PCE when the Ta_2O_5 content reached a certain level. Therefore, the effect of Ta_2O_5 in CBLs to the overall PCE could be taken as a similar phenomenon for various types of inverted OPVs.

Furthermore, the power conversion efficiency of the unencapsulated inverted OPVs was periodically measured for 42 days to monitor their long-term stability in air (Fig. 9). All devices retain around 100% of the magnitude of their original power conversion efficiency after being exposed to ambient conditions for 42 days. This explicitly demonstrates the superior air stability of inverted OPVs.

Table 4 *I–V* characteristics of inverted OPVs with various Ta_2O_5–ZnO CBLs (BHJ active layer: PSEHTT:$PC_{71}BM$)

PSEHTT:PCBM	V_{oc} (V)	J_{sc} (mA cm^{-2})	FF	Efficiency (%)
Pure ZnO	0.67	12.04	0.656	5.29
6% Ta_2O_5	0.67	12.17	0.675	5.51
12% Ta_2O_5	0.68	12.07	0.689	5.61
18% Ta_2O_5	0.67	12.36	0.667	5.57
24% Ta_2O_5	0.68	10.77	0.171	1.25
30% Ta_2O_5	0.77	0.05	0.482	0.002

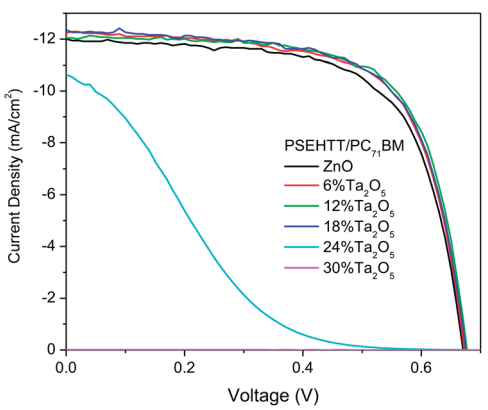

Fig. 8 The *I–V* curve at 1 sun and dark condition with various Ta_2O_5–ZnO films as the cathodic buffer layer (BHJ active layer: PSEHTT:$PC_{71}BM$).

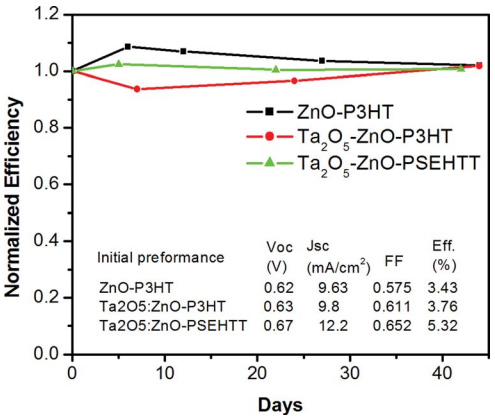

Fig. 9 The long term stability of inverted OPVs with ZnO or Ta_2O_5–ZnO films as the cathodic buffer layer; the devices were stored in ambient conditions.

Conclusions

Ta_2O_5–ZnO films have been fabricated and demonstrated as cathodic buffer layers in inverted polymer solar cells for improved power conversion efficiency. The device performance was found to be strongly dependent on the amount of Ta_2O_5 in CBLs. The data suggested that with Ta present in CBLs, Ta–O–Zn bonding was formed, which is beneficial to the overall PCE. Moreover, some surface gain boundaries might be covered by Ta_2O_5 resulting in fewer oxygen adsorbing sites. Ta_2O_5, famous for its high dielectric constant, might also provide a self-built electric field on the interface between the HBJ active layer and CBL to reduce the electron recombination resulting in enhanced power conversion efficiency. However, a continued increase in the amount of Ta_2O_5 in ZnO film led to lower electron mobility and low crystallinity of CBLs. In the present study, it was found that the power conversion efficiency of the P3HT/$PC_{61}BM$ system increases from 3.7% to 4.12%, presenting an 11% enhancement, and for the PSEHTT/$PC_{71}BM$ system, the power conversion efficiency increases from 5.29% to 5.61%. Moreover, the long-term stability of the unencapsulated inverted OPVs was periodically measured for 42 days. All the devices retained around 100% of their original power conversion efficiencies.

Acknowledgements

This work is supported in part by the U.S. Department of Energy, Office of Basic Energy Sciences, Division of Materials Sciences, under Award no. DE-FG02-07ER46467.

Notes and references

1 R. Po, C. Carbonera, A. Bernardi and N. Camaioni, The role of buffer layers in polymer solar cells, *Energy Environ. Sci.*, 2011, **4**(2), 285, DOI: 10.1039/c0ee00273a.

2 G. Yu, J. Gao, J. C. Hummelen, F. Wudl and A. J. Heeger, Polymer Photovoltaic Cells: Enhanced Efficiencies *via* a

Network of Internal Donor–Acceptor Heterojunctions, *Science*, 1995, **270**(5243), 1789–1791, DOI: 10.1126/science.270.5243.1789.

3 W. Ma, C. Yang, X. Gong, K. Lee and A. J. Heeger, Thermally Stable, Efficient Polymer Solar Cells with Nanoscale Control of the Interpenetrating Network Morphology, *Adv. Funct. Mater.*, 2005, **15**(10), 1617–1622, DOI: 10.1002/adfm.200500211.

4 H.-Y. Chen, J. Hou, S. Zhang, *et al.*, Polymer solar cells with enhanced open-circuit voltage and efficiency, *Nat. Photonics*, 2009, **3**(11), 649–653, DOI: 10.1038/nphoton.2009.192.

5 T. Ameri, G. Dennler, C. Lungenschmied and C. J. Brabec, Organic tandem solar cells: A review, *Energy Environ. Sci.*, 2009, **2**(4), 347, DOI: 10.1039/b817952b.

6 Y. Liang, Z. Xu, J. Xia, *et al.*, For the bright future-bulk heterojunction polymer solar cells with power conversion efficiency of 7.4%, *Adv. Mater.*, 2010, **22**(20), E135–E138, DOI: 10.1002/adma.200903528.

7 W. Li, K. H. Hendriks, W. S. C. Roelofs, Y. Kim, M. M. Wienk and R. A. J. Janssen, Efficient small bandgap polymer solar cells with high fill factors for 300 nm thick films, *Adv. Mater.*, 2013, **25**(23), 3182–3186, DOI: 10.1002/adma.201300017.

8 D. Mühlbacher, M. Scharber, M. Morana, *et al.*, High Photovoltaic Performance of a Low-Bandgap Polymer, *Adv. Mater.*, 2006, **18**(21), 2884–2889, DOI: 10.1002/adma.200600160.

9 Y. He, H.-Y. Chen, J. Hou and Y. Li, Indene-C(60) bisadduct: a new acceptor for high-performance polymer solar cells, *J. Am. Chem. Soc.*, 2010, **132**(4), 1377–1382, DOI: 10.1021/ja908602j.

10 G. Li, V. Shrotriya, J. Huang, *et al.*, High-efficiency solution processable polymer photovoltaic cells by self-organization of polymer blends, *Nat. Mater.*, 2005, **4**(11), 864–868, DOI: 10.1038/nmat1500.

11 G. Heywang and F. Jonas, Poly(alkylenedioxythiophene)s—new, very stable conducting polymers, *Adv. Mater.*, 1992, **4**(2), 116–118, DOI: 10.1002/adma.19920040213.

12 F. Zhang, M. Johansson, M. R. Andersson, J. C. Hummelen and O. Inganäs, Polymer Photovoltaic Cells with Conducting Polymer Anodes, *Adv. Mater.*, 2002, **14**(9), 662–665, DOI: 10.1002/1521-4095(20020503)14:9<662::AID-ADMA662>3.0.CO;2-N.

13 T. Yang, M. Wang, Y. Cao, *et al.*, Polymer Solar Cells with a Low-Temperature-Annealed Sol–Gel-Derived MoO_x Film as a Hole Extraction Layer, *Adv. Energy Mater.*, 2012, **2**(5), 523–527, DOI: 10.1002/aenm.201100598.

14 Y.-J. Cheng, F.-Y. Cao, W.-C. Lin, C.-H. Chen and C.-H. Hsieh, Self-Assembled and C.-L. Fullerene Interlayer on Titanium Oxide for Highly Efficient Inverted Polymer Solar Cells, *Chem. Mater.*, 2011, **23**(6), 1512–1518, DOI: 10.1021/cm1032404.

15 S. K. Hau, H.-L. Yip, H. Ma and A. K.-Y. Jen, High performance ambient processed inverted polymer solar cells through interfacial modification with a fullerene self-assembled monolayer, *Appl. Phys. Lett.*, 2008, **93**(23), 233304, DOI: 10.1063/1.3028094.

16 J. You, C.-C. Chen, Z. Hong, *et al.*, 10.2% power conversion efficiency polymer tandem solar cells consisting of two identical sub-cells, *Adv. Mater.*, 2013, **25**(29), 3973–3978, DOI: 10.1002/adma.201300964.

17 J. S. Kim, R. H. Friend and F. Cacialli, Improved operational stability of polyfluorene-based organic light-emitting diodes with plasma-treated indium–tin-oxide anodes, *Appl. Phys. Lett.*, 1999, **74**(21), 3084, DOI: 10.1063/1.124069.

18 K. Kawano, R. Pacios, D. Poplavskyy, J. Nelson, D. D. C. Bradley and J. R. Durrant, Degradation of organic solar cells due to air exposure, *Sol. Energy Mater. Sol. Cells*, 2006, **90**(20), 3520–3530, DOI: 10.1016/j.solmat.2006.06.041.

19 M. P. De Jong, L. J. van IJzendoorn and M. J. A. de Voigt, Stability of the interface between indium–tin-oxide and poly(3,4-ethylenedioxythiophene)/poly(styrenesulfonate) in polymer light-emitting diodes, *Appl. Phys. Lett.*, 2000, **77**(14), 2255, DOI: 10.1063/1.1315344.

20 S. K. Hau, H.-L. Yip and A. K.-Y. Jen, A Review on the Development of the Inverted Polymer Solar Cell Architecture, *Polym. Rev.*, 2010, **50**(4), 474–510, DOI: 10.1080/15583724.2010.515764.

21 G. Li, C.-W. Chu, V. Shrotriya, J. Huang and Y. Yang, Efficient inverted polymer solar cells, *Appl. Phys. Lett.*, 2006, **88**(25), 253503, DOI: 10.1063/1.2212270.

22 Y. Zhou, H. Cheun, W. J. Potscavage Jr, C. Fuentes-Hernandez, S.-J. Kim and B. Kippelen, Inverted organic solar cells with ITO electrodes modified with an ultrathin Al2O3 buffer layer deposited by atomic layer deposition, *J. Mater. Chem.*, 2010, **20**(29), 6189, DOI: 10.1039/c0jm00662a.

23 Z. Liang, Q. Zhang, O. Wiranwetchayan, *et al.*, Effects of the Morphology of a ZnO Buffer Layer on the Photovoltaic Performance of Inverted Polymer Solar Cells, *Adv. Funct. Mater.*, 2012, **22**(10), 2194–2201, DOI: 10.1002/adfm.201101915.

24 J. H. Lee, S. Cho, A. Roy, H.-T. Jung and A. J. Heeger, Enhanced diode characteristics of organic solar cells using titanium suboxide electron transport layer, *Appl. Phys. Lett.*, 2010, **96**(16), 163303, DOI: 10.1063/1.3409116.

25 J. Liu, K.-L. Choy and X. Hou, Charge transport in flexible solar cells based on conjugated polymer and ZnO nanoparticulate thin films, *J. Mater. Chem.*, 2011, **21**(6), 1966, DOI: 10.1039/c0jm02184a.

26 A. Hayakawa, O. Yoshikawa, T. Fujieda, K. Uehara and S. Yoshikawa, High performance polythiophene/fullerene bulk-heterojunction solar cell with a TiO_x hole blocking layer, *Appl. Phys. Lett.*, 2007, **90**(16), 163517, DOI: 10.1063/1.2730746.

27 T. Kuwabara, Y. Kawahara, T. Yamaguchi and K. Takahashi, Characterization of inverted-type organic solar cells with a ZnO layer as the electron collection electrode by ac impedance spectroscopy, *ACS Appl. Mater. Interfaces*, 2009, **1**(10), 2107–2110, DOI: 10.1021/am900446x.

28 J. Gilot, M. M. Wienk and R. A. J. Janssen, Double and triple junction polymer solar cells processed from solution, *Appl. Phys. Lett.*, 2007, **90**(14), 143512, DOI: 10.1063/1.2719668.

29 J.-Y. Chen, F.-C. Hsu, Y.-M. Sung and Y.-F. Chen, Enhanced charge transport in hybrid polymer/ZnO-nanorod solar cells assisted by conductive small molecules, *J. Mater. Chem.*, 2012, **22**(31), 15726, DOI: 10.1039/c2jm31605f.

30 L.-M. Chen, Z. Hong, G. Li and Y. Yang, Recent Progress in Polymer Solar Cells: Manipulation of Polymer:Fullerene Morphology and the Formation of Efficient Inverted Polymer Solar Cells, *Adv. Mater.*, 2009, **21**(14–15), 1434–1449, DOI: 10.1002/adma.200802854.

31 S. K. Hau, Y.-J. Cheng, H.-L. Yip, Y. Zhang, H. Ma and A. K.-Y. Jen, Effect of Chemical Modification of Fullerene-Based Self-Assembled Monolayers on the Performance of Inverted Polymer Solar Cells, *ACS Appl. Mater. Interfaces*, 2010, **2**(7), 1892–1902, DOI: 10.1021/am100238e.

32 T. Shirakawa, T. Umeda, Y. Hashimoto, A. Fujii and K. Yoshino, Effect of ZnO layer on characteristics of conducting polymer/C 60 photovoltaic cell, *J. Phys. D: Appl. Phys.*, 2004, **37**(6), 847–850, DOI: 10.1088/0022-3727/37/6/007.

33 C.-T. Chen, F.-C. Hsu, S.-W. Kuan and Y.-F. Chen, The effect of C60 on the ZnO-nanorod surfacein organic–inorganic hybrid photovoltaics, *Sol. Energy Mater. Sol. Cells*, 2011, **95**(2), 740–744, DOI: 10.1016/j.solmat.2010.10.015.

34 R. Thitima, C. Patcharee, S. Takashi and Y. Susumu, Efficient electron transfers in ZnO nanorod arrays with N719 dye for hybrid solar cells, *Solid-State Electron.*, 2009, **53**(2), 176–180, DOI: 10.1016/j.sse.2008.10.014.

35 Y. Zhou, C. Fuentes-Hernandez, J. Shim, *et al.*, A universal method to produce low-work function electrodes for organic electronics, *Science*, 2012, **336**(6079), 327–332, DOI: 10.1126/science.1218829.

36 X. Bulliard, S.-G. Ihn, S. Yun, *et al.*, Enhanced Performance in Polymer Solar Cells by Surface Energy Control, *Adv. Funct. Mater.*, 2010, **20**(24), 4381–4387, DOI: 10.1002/adfm.201000960.

37 S. Park, S. J. Tark, J. S. Lee, H. Lim and D. Kim, Effects of intrinsic ZnO buffer layer based on P3HT/PCBM organic solar cells with Al-doped ZnO electrode, *Sol. Energy Mater. Sol. Cells*, 2009, **93**(6–7), 1020–1023, DOI: 10.1016/j.solmat.2008.11.033.

38 A. K. K. Kyaw, X. Sun, D. W. Zhao, S. T. Tan, Y. Divayana and H. V. Demir, Improved Inverted Organic Solar Cells With a Sol–Gel Derived Indium-Doped Zinc Oxide Buffer Layer, *IEEE J. Sel. Top. Quantum Electron.*, 2010, **16**(6), 1700–1706, DOI: 10.1109/JSTQE.2009.2039200.

39 T. Z. Oo, R. Devi Chandra, N. Yantara, *et al.*, Zinc Tin Oxide (ZTO) electron transporting buffer layer in inverted organic solar cell, *Org. Electron.*, 2012, **13**(5), 870–874, DOI: 10.1016/j.orgel.2012.01.011.

40 J.-L. Lan, Z. Liang, Y.-H. Yang, F. S. Ohuchi, S. A. Jenekhe and G. Cao, The effect of $SrTiO_3$:ZnO as cathodic buffer layer for inverted polymer solar cells, *Nano Energy*, 2014, **4**, 140–149, DOI: 10.1016/j.nanoen.2013.12.010.

41 M. Thambidurai, J. Y. Kim, C. Kang, *et al.*, Enhanced photovoltaic performance of inverted organic solar cells with In-doped ZnO as an electron extraction layer, *Renewable Energy*, 2014, **66**, 433–442, DOI: 10.1016/j.renene.2013.12.031.

42 Z. L. Wang, Towards Self-Powered Nanosystems: From Nanogenerators to Nanopiezotronics, *Adv. Funct. Mater.*, 2008, **18**(22), 3553–3567, DOI: 10.1002/adfm.200800541.

43 X. Du, Z. Mei, Z. Liu, *et al.*, Controlled Growth of High-Quality ZnO-Based Films and Fabrication of Visible-Blind and Solar-Blind Ultra-Violet Detectors, *Adv. Mater.*, 2009, **21**(45), 4625–4630, DOI: 10.1002/adma.200901108.

44 L. Schmidt-Mende and J. L. MacManus-Driscoll, ZnO – nanostructures, defects, and devices, *Mater. Today*, 2007, **10**(5), 40–48, DOI: 10.1016/S1369-7021(07)70078-0.

45 Y. Bai, H. Yu, Z. Li, R. Amal, G. Q. M. Lu and L. Wang, *In situ* growth of a ZnO nanowire network within a TiO_2 nanoparticle film for enhanced dye-sensitized solar cell performance, *Adv. Mater.*, 2012, **24**(43), 5850–5856, DOI: 10.1002/adma.201201992.

46 H. Cheun, C. Fuentes-Hernandez, Y. Zhou, *et al.*, Electrical and Optical Properties of ZnO Processed by Atomic Layer Deposition in Inverted Polymer Solar Cells, *J. Phys. Chem. C*, 2010, **114**(48), 20713–20718, DOI: 10.1021/jp106641j.

47 K. M. Noone, S. Subramaniyan, Q. Zhang, G. Cao, S. A. Jenekhe and D. S. Ginger, Photoinduced Charge Transfer and Polaron Dynamics in Polymer and Hybrid Photovoltaic Thin Films: Organic vs Inorganic Acceptors, *J. Phys. Chem. C*, 2011, **115**(49), 24403–24410, DOI: 10.1021/jp207514v.

48 S. Yildirim, K. Ulutas, D. Deger, E. O. Zayim and I. Turhan, Dielectric properties of sol–gel derived Ta_2O_5 thin films, *Vacuum*, 2005, **77**(3), 329–335, DOI: 10.1016/j.vacuum.2004.12.002.

49 F. Rubio, J. Denis, J. M. Albella and J. M. Martinez-Duart, Sputtered Ta_2O_5 antireflection coatings for silicon solar cells, *Thin Solid Films*, 1982, **90**(4), 405–408, DOI: 10.1016/0040-6090(82)90545-4.

50 S. Ezhilvalavan and T. Y. Tseng, Preparation and properties of tantalum pentoxide (Ta_2O_5) thin films for ultra large scale integrated circuits (ULSIs) application – A review, *J. Mater. Sci.: Mater. Electron.*, 1999, **10**(1), 9–31, DOI: 10.1023/A:1008970922635.

51 D. Briggs, *Handbook of X-ray Photoelectron Spectroscopy*, ed. C. D. Wanger, W. M. Riggs, L. E. Davis, J. F. Moulder and G. E. Muilenberg, Perkin-Elmer Corp., Physical Electronics Division, Eden Prairie, Minnesota, USA, 1979, pp. 190, *Surf. Interface Anal.*, 1981, **3**(4), DOI: 10.1002/sia.740030412.

52 V. D. Mihailetchi, J. K. J. van Duren, P. W. M. Blom, *et al.*, Electron Transport in a Methanofullerene, *Adv. Funct. Mater.*, 2003, **13**(1), 43–46, DOI: 10.1002/adfm.200390004.

53 A. J. Moulson and J. M. Herbert, *Electroceramics: Materials, Properties, Applications*, Wiley, 2nd edn, 2003, http://www.wiley.com/WileyCDA/WileyTitle/productCd-0471497487.html, accessed March 5, 2014.

54 O. Wiranwetchayan, Z. Q. Liang, Q. F. Zhang, G. Z. Cao and P. Singjai, The Role of Oxide Thin Layer in Inverted Structure Polymer Solar Cells, *Mater. Sci. Appl.*, 2011, **02**(12), 1697–1701, DOI: 10.4236/msa.2011.212226.

55 F. Verbakel, S. C. J. Meskers and R. A. J. Janssen, Electronic memory effects in diodes from a zinc oxide nanoparticle–polystyrene hybrid material, *Appl. Phys. Lett.*, 2006, **89**(10), 102103, DOI: 10.1063/1.2345612.

56 S. Subramaniyan, H. Xin, F. S. Kim, S. Shoaee, J. R. Durrant and S. A. Jenekhe, Effects of Side Chains on Thiazolothiazole-Based Copolymer Semiconductors for High Performance Solar Cells, *Adv. Energy Mater.*, 2011, **1**(5), 854–860, DOI: 10.1002/aenm.201100215.

